Boundary layer isentropic and kinematic trajectories during the August 1993 North Atlantic Regional Experiment Intensive

Roland R. Draxler (JGR, Vol 101, No. D22, Pg 29255-29268, Dec. 20, 1996)

Air Resources Laboratory, NOAA, Silver Spring, Maryland

Abstract. Four per day backward trajectories were computed from Chebogue Point, Nova Scotia, for the month of August 1993 using two different three-dimensional approaches: diagnostic vertical velocity fields (kinematic) and an isentropic assumption. Essentially, 90% of all the kinematic-isentropic trajectory pairs were displaced within ±75 hPa of each other and differed in the horizontal by about 10% of the travel distance. The greatest vertical displacement differences occurred with flow from the northwest and only three time periods were associated with the greatest displacements; a cyclonic system was to the north of the trajectory starting location in each case. Precipitation was associated with two of these events. A moist isentropic departure was computed for both kinematic and isentropic cases and departures were typically about 5EK. Comparison of CO measurements and upwind trajectories suggested by temporal groupings of trajectories were consistent with transport from major urban areas. However, the peak measured CO values seemed to occur more frequently with flow transition periods, when trajectory uncertainty is the greatest.

1. Introduction

Lagrangian trajectory methods have enjoyed considerable popularity with the atmospheric chemistry community as an approach to determine the potential source regions of measured airborne pollutants. Most computational methods use observed or model analyzed winds to compute the horizontal advection component and usually one of three assumptions to compute the vertical component of the trajectory motion. These three assumptions are that the trajectory remains on a surface of constant pressure (isobaric), the trajectory follows a surface of constant potential temperature (isentropic), or the trajectory moves with the vertical velocity wind fields (kinematic) generated by a diagnostic or prognostic meteorological model.

There are many recent examples in the literature of all three approaches. The kinematic approach was used by *Akeredolu et al*. [1994] to determine Arctic trace metal fluxes; *Fontan et al*. [1992] to determine the sources of particulate pollutants in central Africa; *Cheng et al*. [1993] to compute a gridded array of potential source regions for sulfate transport; *Mueller* [1994] to determine the sources of high-ozone episodes at Great Smoky Mountains National Park; *Taguchi* [1994] to compute interhemispheric exchanges in the troposphere; *Moy et al*. [1994] to determine origins of polluted and clean air at Shenandoah National Park; and *Olson and Oikawa* [1989] to estimate transboundary pollutant fluxes. The isobaric approach was used by *Stohl and Kromp-Kolb* [1994] to determine ozone source regions for Vienna, Austria; *Oram*

and Penkett [1994] to attribute methyl iodide concentrations in England to emissions from the Atlantic Ocean; *Swap et al.* [1992] to compute the flux of Saharan dust to the Amazon Basin; and *Lowenthal et al.* [1992] to attribute fine particles measured at Hawaii to the Kuwait oil fires. Isentropic methods were employed by *Klemm et al.* [1994] to determine the air mass history of fog at a New England coastal site; *Oltmans and Levy* [1994] to determine ozone transport to a remote network of monitoring sites; *Hahn et al.* [1992] to determine air mass origins at Mauna Loa Observatory; *Paluch et al.* [1992] to determine the source of polluted air measured over the eastern Pacific; *Shipman et al.* [1992] to determine air mass sources to the Arctic region of Alaska; *Lee et al.* [1994] to determine sources of total nitrate measured at Mauna Loa; and *Andreae et al.* [1994] to correlate haze layers over the South Atlantic with transport from Africa and South America. These are only some of the more recent examples. However, it is sufficient to say that trajectory techniques remain popular, with no particular consensus on methodology.

In a few analyses, different trajectory methods were compared with each other. *Artz et al.* [1985] compared an isentropic model with a model using boundary layer averaged winds and determined that the only significant divergence between the methods occurred near frontal regions. *Harris* [1992] examined the difference between isobaric and isentropic methods over Antarctica and determined that the two methods diverged the most when the flow was over the colder portions of the Antarctic sheet. This resulted in a more accurate depiction of the flow by the isentropic calculation, which properly accounted for the vertical component of the flow over the cold air. *Stunder et al.* [1990] computed source regions for North Atlantic shipboard air samples using both isentropic and isobaric techniques and found both yielded similar source region distributions. When analyzing the source of airborne lead particulate, *Mukai et al.* [1994] found that isobaric trajectories were superior to dry isentropic ones due to the frequent passage of fronts during the study period. *Knudsen and Carver* [1994] compared the sensitivity of stratospheric isentropic trajectories to various temporal and spatial data resolutions and to the actual path of a balloon tracked for 2 days. Errors were small, about 12% of the travel distance, and they were attributed to the difference between real and analyzed winds. However, when they tried to develop an objective method of determining trajectory error, through the conservation of potential vorticity (PV), they found that due to accumulations in trajectory error, PV changed too much to be useful except in the most dramatic cases. *Martin et al.* [1987] compared the kinematic and isobaric approaches and generally found differences to be small within the first 48 hours. However, during moist convection conditions and for boundary layer trajectories during cyclonic regimes, differences between the two methods could be substantial. *Kahl et al.* [1989] compared kinematic, isobaric, and isentropic approaches and concluded that the model's sensitivity to the

input data resulted in greater trajectory uncertainties than the vertical motion parameterization. Using an isentropic model *Pickering et al.* [1994] found large vertical displacements between model simulations using different input meteorological fields over the data sparse South Atlantic.

One common element among many of the above citations is that the choice of computational method is usually limited to a single available model. Presumably three-dimensional approaches are superior to more restricted methods. This was demonstrated by E.F. Danielsen in his 1961 classic paper showing how isobaric techniques were inadequate when compared with three-dimensional isentropic calculations. There is no point revisiting that question again; however, there are a variety of three-dimensional computational methods in use and it would be interesting to examine results from the two most common methods as applied to an actual experimental situation. In this analysis boundary layer (BL) trajectories computed using a three-dimensional kinematic approach will be compared with comparable trajectories computed using a "quasi-isentropic" assumption for a period corresponding to surface and airborne atmospheric chemistry measurements made during August 1993 in support of the North Atlantic Regional Experiment (NARE) [*Fehsenfeld et al.*, this issue].

Transport is perhaps more difficult to model in the BL than in the upper troposphere or stratosphere due to significant amounts of moisture and the diabatic factors driving the growth and dissipation of the BL itself. One underlying assumption is that the three-dimensional velocity fields generated by a meteorological forecast model contain all the adiabatic as well as diabatic components to the vertical motion. Many of the citations using dry isentropic approaches frequently are preceded by qualifying statements regarding the exclusion of situations that have large diabatic components: convective boundary layers, cloud coverage, and areas of precipitation. These factors should not be a problem for application to upper tropospheric and stratospheric transport. However, these limitations, although stated, are frequently overlooked in BL transport problems. Some of these factors will be examined in the following sections.

2. Trajectory Methods

The interest here is primarily to compare kinematic and isentropic computational approaches for a location and period where some relevant conclusions can be reached. There is no intention to suggest one particular model over another. However, it is necessary to confine the comparison to one model, with a minimum amount of modification to handle different three-dimensional approaches. This ensures that differences in the computational results are only due to factors under consideration and are performed on the same meteorological database.

As with many models using gridded meteorological data fields, the trajectory calculations (HY-SPLIT model) [*Draxler*, 1992] follow a geometric approach. The trajectories' three-dimensional motion is computed from the *u*,*v*, and ? (*dp*/*dt*) component winds output and archived every 2 hours from NOAA's National Meteorological Center's Nested Grid Model (NGM). The time series consists of twice-daily consecutive model forecast fields from +2 hours after initialization to +12 hours. Archives of the 2-hour fields are available since 1991 from the National Climatic Data Center (NCDC reference TD-6140). The fields, an extract from the model's native 90-km grid, are given on a 180-km polar stereographic grid at 10 model sigma levels from 0.982 to 0.434. There are about four levels within the boundary layer. There is no temporal interpolation of the NGM meteorological fields between 2-hour periods and in both the kinematic and isentropic calculations the horizontal advection over the time step ? *t* (1 hour) is calculated as the initial position $\mathbf{X}_0$ to the final position

$$\mathbf{X}_2 = \mathbf{X}_0 + 0.5(\mathbf{V}_0 + \mathbf{V}_1) ? t , \quad (1)$$

where $\mathbf{V}_0$ is the horizontal wind vector at the initial position $\mathbf{X}_0$ and $\mathbf{V}_1$ is the wind at position

$$\mathbf{X}_0 + \mathbf{V}_0 ? t. \quad (2)$$

This method is a simple first-order approximation to account for curvature in the wind field. The trajectory's final horizontal position at an arbitrary level P_0 is the average of the trajectory positions $\mathbf{X}_2$ computed on the model sigma levels below and above the height P_0. In general the trajectory results are insensitive to time step as long as the trajectory displacement in one time step is less than half the grid spacing. The meteorological grid spacing of 180 km provides a wide range of stable time steps for the generally slower BL trajectories.

In the standard calculation, called kinematic for the discussion in this paper, the new vertical position or pressure of the particle at $\mathbf{X}_2$ is given by

$$P_2 = P_0 + 0.5(? _0 + ? _1) ? t. \quad (3)$$

The vertical velocity $? _1$ is defined at the same position as $\mathbf{V}_1$. A linear interpolation from the data grid is used to define meteorological variables at the particle position.

The configuration of the isentropic version of the model is considerably simplified over the more sophisticated approaches evaluated by *Merrill et al.* [1986]. However, in order to utilize the same code and minimize differences due to computational techniques and input data variations, the isentropic version of the calculation leaves all the kinematic computational methods intact. Only the vertical velocity field is replaced by a velocity required to keep a parcel on the same isentropic stream function. One computational restriction of the model is that it should be able to run on a desktop PC with

conventional memory restrictions, hence it limits concurrent availability of meteorological fields to one time period. Since the meteorological fields are available at a 2-hour frequency, and to be consistent with the kinematic calculation, local time derivatives are assumed to be zero, and therefore for isentropic motion the vertical velocity fields can be simplified such that

$$w_i = [\, -u\, \partial?/\partial x - v\, \partial?/\partial y \,]\, [\, \partial?/\partial z \,]^{-1}\,, \qquad (4)$$

where the Montgomery stream function? equals C_pT+gz, and C_p is the specific heat at constant pressure, T is the air temperature, g is the acceleration of gravity, and z is height. The approach is equivalent to following the potential temperature surfaces because the isentropic trajectory must be parallel to the stream functions on a potential temperature surface in geostrophic flow. Here w_i (height units) is then converted to ? (pressure units) and used for vertical motion calculations at all grid points where the stability criterion $\partial?/\partial z > 1.0$ is satisfied. At the grid points with excessive BL instability, the original NGM diagnostic vertical velocity is retained. During the August 1993 period, 5.9% of the isentropic trajectory computational times were affected by the BL instability criterion. Note that the above equations are only quasi-isentropic because they do not require any properties to be conserved over the duration of the trajectory. There will always be differences due to the accumulation of computational errors as well as occasional discontinuity introduced with each new meteorological forecast data field. Although neither the kinematic nor isentropic computational technique is optimized to avoid these problems, it does permit a comparison of the two approaches using the same data fields and computational methods.

3. Trajectory Statistics

Although NARE consisted of a variety of measurements at several locations, only calculations of backward trajectories from Chebogue Point (43.74EN, 66.12EW), near Yarmouth, Nova Scotia, for the month of August 1993, will be used in the evaluation. The other continuous monitoring site, on Sable Island, was too near the edge of the meteorological data grid. Trajectories were started 4 times per day (0, 6, 12, and 18 hours UTC) from a height of 10 m AGL. Although the computations were made 5 days upwind, the statistical analysis and graphics only used results from the first 48 hours. Endpoint positions were generated using both the isentropic and kinematic methods.

Both horizontal and vertical displacement statistics were calculated for each isentropic and kinematic trajectory pair. The Relative Horizontal Trajectory Difference (RHTD),

$$\mathrm{RHTD} = 2\, {}_i\mathbf{X_i} - \mathbf{X_k}\, [\, \mathbf{X_i} + \mathbf{X_k} - 2\, \mathbf{X}_0 \,]^{-1}, \qquad (5)$$

is calculated for each endpoint-position pair. The position

vector **X** is identified by the subscripts **i** and **k** for the isentropic and kinematic trajectories, while $\mathbf{X}_0$ indicates the position of the trajectory origin. The second term represents the average upwind distance of the two trajectories. The total vertical displacement (TVD) between the methods is simply defined as the pressure difference between the trajectories

$$\text{TVD} = P_i - P_k, \tag{6}$$

where a negative TVD indicates that the isentropic trajectory has a lower pressure and hence is at a higher elevation than its kinematic counterpart.

The RHTD and TVD are calculated for each trajectory pair as the average of all endpoints between 24 and 48 hours upwind. The averaging provides a single value to be identified with each trajectory pair. Farther upwind (>48 hours), the departures, both horizontal and vertical, become so great that the differences become less significant because the individual trajectories are usually in different flow regimes. Owing to the accumulation of uncertainties, *Kahl et al.* [1989] questioned trajectory accuracy much beyond 3 days travel time.

The relationship between TVD and RHTD is shown in Figure 1. The abscissa is expressed in pressure unit bins of 25 hPa. The ordinate value gives the average RHTD for all trajectory pairs in a TVD bin. Not surprisingly, the greatest horizontal differences are associated with the greatest vertical displacements between trajectories. The trajectory count in the 25 hPa bins is shown in Figure 2 and the results indicate a clear separation between the bulk of the cases where the differences between the isentropic and kinematic calculation are negligible, and those few cases of great displacement in which the isentropic trajectory rises well above the kinematic one. Essentially, 90% of all trajectory pairs fall in the ±75 hPa displacement range with horizontal errors less than 10% of the travel distance. The distribution is skewed toward upward displacement bias due to the restriction of the ground surface and greater vertical motion associated with the isentropic calculation.

These results are only representative for the time and location of the simulations. Summer meteorological conditions are expected to be more barotropic and one would expect differences to be small. Furthermore, the water surfaces surrounding the site would reduce diurnal BL variations. The results are consistent with those of *Haagenson and Sperry* [1989] who found that the bulk (90%) of their BL trajectories had vertical motions of 100 hPa per day or less.

4. Trajectory Views

The previous illustrations showed that most of the trajectories were very similar, 50% were within ±25 hPa and 90% were within ±75 hPa. Certainly, those within ±25 hPa can be considered to be almost identical because the vertical

resolution of the meteorological data field is of that order. However, differences of >100 hPa, or about 1 km, may place many of these trajectory pairs in different flow regimes. The similarities and differences can be seen in Figure 3 for the kinematic calculation and Figure 4 for the isentropic calculation. Only trajectories in which the kinematic-isentropic pair had a displacement difference of <100 hPa are shown. These cases represent the breakpoint in the distribution (Figure 2). The small box below each map shows the vertical projection of each trajectory below its path on the map. North-south trajectories will tend to be clustered together, while east-west trajectories will be more drawn out. This factor is important as the bulk of the trajectories have either a north or south main component. These trajectories show little vertical displacement from each other. Only the trajectories originating from the northwest, those with most of their vertical projection on the left side of the illustration, show any appreciable differences (although still less than 100 hPa) and those differences seem to occur primarily at the furthest upwind region. Those isentropic trajectories seem to have more upward curvature while the kinematic ones have a small downward component.

Another interesting feature is that except for a few single trajectories, both horizontal distributions look almost identical, a result consistent with RHTDs of less than 10%. Clearly clustering or sector analysis of these trajectories would yield comparable results for either the kinematic or isentropic approach. In this particular period, important source regions can be identified without resort to more sophisticated approaches. The relationship between trajectory clusters, or upwind source regions, and chemical measurements, is addressed later in this paper and elsewhere in this issue; however, general conclusions from these analyses should be similar regardless of the trajectory calculation methods employed.

The uncertainty regarding the vertical component of the transport is illustrated by showing those few trajectory pairs with the greatest vertical differences. There are only nine trajectory pairs in which the 24 to 48 hour average displacement was greater than 100 hPa. The kinematic trajectories are shown in Figure 5 and the isentropic ones in Figure 6. Note that they are all from the west or northwest, comparable to the trajectories with greatest vertical differences shown in Figures 3 and 4. Although the differences in the vertical component are on the order of 200-300 hPa, the horizontal paths are remarkably similar, indicating little vertical shear of the horizontal wind. The corresponding RHTDs of 20 to 40% (Figure 1) would still yield comparable source region information when compared with the range of upwind directions permitted in a typical trajectory cluster. Regardless of the actual magnitude of the TVD between methods, it is clear that the differences occur primarily with flow from the northwest.

5. Synoptic Situation

The issue of larger vertical displacement between trajectories with northwest flow suggests that there may be problems in dealing with subsidence cases. It seems unlikely, but one might speculate that the isentropic approach would more accurately capture the slope of the potential temperature surfaces near the ground. In the kinematic approach, mass conservation suggests that the vertical velocity must vanish near the ground or perhaps just above the BL during a strong subsidence event. A simple calculation of the average absolute vertical velocities over Chebogue (nearest NGM grid point) during August shows that the magnitude drops from 4.7 hPa h^{-1} at midatmosphere to 1.2 hPa h^{-1} at the lowest sigma level, about 200 m above ground. Since near-ground kinematic vertical motions are only 25% of those in the midatmosphere, except for the strongest of vertical motion synoptic cases, it would be very difficult to get a kinematic trajectory out of the BL.

An examination of those trajectories with the greatest differences shows that although there are nine trajectories with large differences in vertical displacement, they only represent three independent meteorological periods, which are summarized in Table 1. Period A extends beyond a full day (5 trajectories), while periods C and D consist of only two trajectories each (over period of 12 hours). The synoptic situation during these periods is illustrated by the mean sea level pressure (MSLP) maps in Figure 7 for the beginning of each period. Owing to the extended duration of period A, the MSLP at the end of the period (panel B) is shown as well. Remarkably, all three periods represent comparable initial situations; a high-pressure center in the upper Midwest (Ohio) and a low-pressure center, near or approaching Newfoundland, Canada. The region around the trajectory origin site, the southern tip of Nova Scotia, has winds generally from the west or northwest, and is consistently near a frontal region or low-pressure trough. The greatest difference between these three situations appears to be the magnitude of the pressure gradient over Nova Scotia with the slowest transport occurring during situation A. The three periods represent all the trajectories previously shown in Figures 5 and 6, where the five short trajectories to the west represent the slow transport of period A, while the faster more northwesterly pairs represent the flow during periods C and D. *Haagenson and Sperry* [1989], using a dry isentropic model, found that most upwind trajectory ascent, in that geographic region, was associated with a starting position located southeast of an 850 hPa low. This would be comparable to a trough near the release location, because the upper level low is usually located to the west of the surface trough.

In the latter two periods C and D, those with nearby fronts, strong winds, and relatively short time during which the vertical transport of the kinematic and isentropic trajectories didn't match well, one can argue that diabatic processes may have played a crucial role. For example, the kinematic and isentropic trajectory pairs shown in Figures 8 and 9, only 6

hours after the end of periods C and D (1200 UTC Aug. 22 and 1800 UTC Aug. 29) show a much better match between calculations than those shown previously in Figures 5 and 6. Similar factors would be important in case A; however, the longer time period and weaker more complex patterns make the case less attractive for analysis.

Although subsidence certainly could be significant upwind of the trajectory starting location and for the trajectories shown in Figures 8 and 9, the major differences in the high vertical displacement cases (Figures 5 and 6) appear to be driven by factors associated with the nearby cyclonic systems. *Haagenson et al*. [1990] analyzed surface tracer concentrations during a winter experiment in the upper Midwest and found that in several of the cases in which ground level concentrations were unexpectedly low, their three-dimensional forward trajectories indicated large-scale vertical motions transporting tracer from the BL to the troposphere. They found vertical displacements to be on the order of 100 hPa to 150 hPa at 1.5 to 2.5 days transport time, comparable to the vertical motions seen in these two examples. However, in both C and D, the NGM predicts precipitation over the trajectory origin point. Regardless of whether precipitation actually occurred, the model fields will reflect the diabatic effects of the predicted rainfall; a dry isentropic backward trajectory should rise higher than its moist counterpart (comparable to the kinematic). It appears that over the month covered by the NARE intensive period, there are broad time bands when the different computational techniques yield comparable results, divided by short baroclinic periods, where the vertical motion assumptions can make a significant difference on the trajectory path.

6. Isentropic Cross Section

One way to examine the trajectory calculation is to show the trajectory with respect to the isentropic surfaces as in Figure 10 (the first trajectory period C) and Figure 11 (trajectory just after the end of the period). These illustrations are not the typical spatial cross section. The abscissa represents upwind time along the trajectory; therefore both space and time vary along the abscissa. The ordinate shows the approximate height of the data levels archived from the NGM model output fields. The trajectory height is indicated each hour by the *X* symbol. Note how in the first simulation (Figure 10) where the kinematic and isentropic trajectories had the most vertical displacement, the potential temperature starts near 290EK and ends near 308EK. The trajectory 12 hours later (Figure 11) stays near the 290EK surface for its entire path. This suggests that the dry adiabatic assumption was more valid for the case shown in Figure 11 than in Figure 10 where the trough was located near the trajectory starting location.

For synoptic case D, the diverging trajectories (Figure 12) start near 300EK and end near 310EK, while those calculated

12 hours later (Figure 13) stay near the 290EK surface for half the time. The large temperature change in the initial value between Figures 12 and 13 in case D suggests a change in air mass. These illustrations show only the isentropic trajectories, however in both Figures 10 and 12, the corresponding kinematic trajectories did not rise as much staying closer to the initial temperature surface.

Although as indicated above there is a suggestion of an air mass change in case D, none of the trajectories (Figures 5 and 6) show marked "kinks" which might indicate an unrealistic passage through a front. Therefore one might suspect that the entire diabatic change along the trajectory may be due to the effects of moisture. In areas of precipitation and clouds, the release of latent heat will increase the potential temperature of the air. However, since a backward or upwind trajectory calculation is being performed, a parcel tagged with a specific temperature (the isentropic trajectory) will pass through colder air and hence must rise upward to maintain that same temperature. This is consistent with the large initial temperature drop between Figures 12 and 13. Furthermore, the MSLP map (Figure 7, panel D) indicated that the front was already to the east at the start of the period.

All back trajectory calculations that make a dry adiabatic assumption will be biased upward in regions of latent heat release. The diabatic term can of course be computed to correct the vertical motion: $d?/dt(M?/Mz)^{-1}$. A moisture change of about 1 g/kg is equivalent to a temperature change of about 3 K or 300 m vertical displacement. Presumably, this is all implicit in the kinematic calculation, where the vertical velocity fields are derived directly from the meteorological model.

Another interesting feature to be found in these cross-section illustrations, discussed briefly earlier, is the effect of the diurnal variations in BL temperature. Generally, between the hours of 1200, 0600 and 0000 (night) the BL temperature structure is well defined, while during the hours of 0000, 1800, and 1200 (day) the isentropic surfaces are nearly vertical in the BL. This is of course well known, and suggests that there could be more of a tendency for isentropic (forward) trajectories to exit the BL during day or night transitions, when the isentropic surfaces are well defined. The warming BL of night to day transition should keep a trajectory near the ground, while a day to night transition suggest that all the pollutant material must become elevated as the boundary layer cools. This process has been observed in the past for a few singular events such as release 3 of the Cross-Appalachian Tracer Experiment (CAPTEX) [*Ferber et al*., 1986]. However, the isentropic trajectories (Figures 11 and 13) from the two driest adiabatic cases show little evidence of any diurnal bias in their motion supporting the initial assumption that most of the upwind vertical motion is associated with subsidence.

7. Moisture

Although not all the components of the trajectory uncer-

tainty can be sufficiently resolved, it is possible to estimate how much of the change in potential temperature along the trajectory is due to effects of changes in moisture content. As suggested by *Taguchi* [1994] this might then provide a quantitative measure of trajectory accuracy. If we assume that all the temperature (T) change with time (t) is due only to moisture then

$$dT/dt = -L/C_p \, dq/dt, \tag{7}$$

where L is the latent heat of condensation, C_p is the specific heat at constant pressure, and q is the specific humidity. If we assume that these changes are in balance then

$$d(\ln T)/dt + -L/C_p \; dq/dt = 0 \tag{8}$$

where T is the potential temperature. The left side of the equation was evaluated at every time step along each trajectory for both the isentropic and kinematic trajectory calculations. Presumably, as long as the trajectory path is in balance with these diabatic processes then the term will remain near zero and hence suggest a more accurate trajectory.

The results are summarized in Figure 14 as the maximum absolute temperature change along each trajectory averaged into 25 hPa vertical displacement categories. For the bulk of the trajectories, where the difference between the isentropic and kinematic calculations is less than 100 hPa, there is no discernable difference in the latent heat contribution to the diabatic tendency between the calculation methods. Temperature changes, or perhaps better called uncertainties, of around 5EK, are consistent with displacement differences of ±75 hPa. Probably most of the uncertainty, or moist isentropic departure, is caused by the accumulation of computational errors due to the limiting assumptions of the model as well as the meteorological data.

The one category with the greatest vertical displacement shows the largest temperature changes between computational methods, with the kinematic calculation showing a slight improvement over the isentropic one. Considering the few cases and large temperature change even for the "good" calculation, one can conclude that all methods are suspect in the vicinity of troughs and frontal regions where the diabatic tendencies will be greater due to additional mixing, moisture, and other effects.

Kuo et al. [1985] analyzed a variety of trajectory methods during a single storm event. He showed that low-level isentropic trajectories differed from their more accurate high-resolution three-dimensional counterparts by 40 to 50 hPa in a 24- to 48-hour travel period. Although he concluded that the isentropic calculation was the best of the three simplifying assumptions (isosigma, isobaric, and isentropic) evaluated, it was not a good assumption in the BL or in regions of precipitation.

8. CO Measurements

Although the issue of pollutant source region attribution for many of the NARE sampling data is addressed elsewhere in this issue, it is worth examining the trajectories with regard to their typical application to source attribution. It was already demonstrated that both computational methods showed comparable horizontal trajectory distributions. However, there were periods when neither method provided reliable results. A simple independent control parameter would be the CO pollutant air concentration measurement at the origin point, Chebogue. CO is typically produced in large quantities from urban areas, is relatively inert, and could provide a reliable tag of transport from polluted urban areas to the remote site. The NOAA Aeronomy Laboratory provided a 5-min time series of continuous CO air concentrations [*Roberts et al*., this issue]. These data were then averaged into 6-hour periods centered about the trajectory starting times so that one average CO air concentration could be associated with each trajectory.

The bulk of the trajectories, shown earlier in Figures 3 and 4, illustrated distinct spatial groupings. However, not evident in those figures was that those groupings were the result of a temporal autocorrelation to the trajectory path; most groups were the result of sequential trajectories in the same direction. After visual examination of all the trajectories within the August period, it was quite clear that consecutive trajectories are not independent and there were abrupt transitions between different flow regimes.

The time series of CO concentrations and the corresponding trajectory groupings are shown in Figure 15. The dotted vertical lines on the illustration represent transition periods between nine different flow regimes, that is, a flow regime is defined very subjectively in that all the trajectories within that consecutive time period are similar. The nine periods are summarized in Table 2, including the average CO air concentration during each period.

The average kinematic trajectory associated with each of the meteorological periods is shown in Figure 16. Some of the obvious directional and CO dependencies are consistent with previous studies [*Moody and Samson*, 1989] that found the transport direction was a better predictor of low pollutant concentration events than the high concentration events. For those few high events, it is interesting to note how the transition periods from one flow regime to the next seem to be associated more with high CO concentrations than the intermediate period when the trajectories are presumed to have some temporal coherence. This is especially dramatic between periods 6-9. Also the three periods (Table 1) in which the kinematic-isentropic trajectory pairs showed large differences are represented here as transition periods as well. As an example it would be very tempting to associate a single high-measurement value and its corresponding trajectory to a particular source region, but the frequent correspondence of

high events with what was found to be generally non adiabatic conditions is suggestive of a much greater trajectory uncertainty. An alternative suggestion [*J.L. Moody*, private communication, 1995] is that enhanced vertical mixing during these baroclinic periods resulted in the breakdown of the marine BL and correspondingly higher CO concentrations at ground level.

The autocorrelation of meteorological parameters is a well-accepted concept. It suggests that the traditional spatial cluster methods, such as pioneered by *Moody and Galloway* [1988] and *Moody and Samson* [1989], should become a two-pass process. On the first pass, trajectories are clustered only in sequential time order, while on the second pass, the time series clusters are merged following traditional spatial methods.

9. Summary and Conclusions

Trajectory methods remain a popular approach for source attribution of atmospheric chemical measurements. It appears that computational methods are frequently chosen based primarily upon the availability of a particular model or data archive. In this analysis the 1993 August NARE Intensive Period was used as a period to test two different three-dimensional trajectory approaches. It is presumed that three-dimensional approaches are superior to two-dimensional assumptions such as isobaric or isosigma trajectories. A transport and dispersion model was modified to permit trajectory calculations using a kinematic method to compute vertical motion from the diagnostic vertical velocity fields from previously analyzed data fields, and a quasi-isentropic approach that replaces the diagnostic vertical velocity with a velocity required to maintain a parcel on the same isentropic stream function. Although the isentropic trajectory method used here was a considerably simplified version of the method first proposed by *Danielsen* [1961] which conserved energy, potential temperature, as well as kinematic properties, it was sufficiently conservative to yield results comparable to using the vertical velocity fields directly from the model in a majority of the cases during the study period.

Four backward trajectories per day were calculated for the entire month of August from Chebogue Point, Nova Scotia, using both computational methods. All were started within the boundary layer to represent typical conditions to associate transport with ground level chemical measurements.

Essentially, 90% of all kinematic-isentropic trajectory pairs are within ±75 hPa of each other and with horizontal differences of less than 10% of the travel distance. The differences between trajectory methods at Chebogue Point were not as large as they might be at other locations or times due to the more barotropic summer meteorological conditions and large area of water surface surrounding the site that would minimize diurnal variations. Horizontal trajectory distributions for either method looked almost identical, indicating that an upwind

source analysis would yield comparable results using either computational approach. There was a tendency for the isentropic trajectories that originated from the northwest to show greater vertical displacement. These are the flow situations in which subsidence is expected to occur with increased frequency.

The remaining 10% of the trajectories, with large vertical departures between the kinematic and isentropic methods, were only associated with three synoptic events. Those cases were all affected by a nearby low pressure or trough and precipitation at the release point. The dry isentropic trajectories did not stay on their potential temperature surfaces. There will be a tendency for dry isentropic back trajectories to rise higher than their moist counterparts. Overall the results are consistent with those of *Haagenson and Sperry* [1989] who found that isentropic trajectories originating within the BL tended to have a greater frequency of upward motion due to the ground barrier as well as the exclusion of moist adiabatic processes in the computations.

It was presumed that the kinematic trajectories should more accurately simulate the three-dimensional motions than the dry isentropic calculation, since the model diagnostic fields explicitly contain all the diabatic effects. In an attempt to determine a quantitative measure of trajectory accuracy a moist adiabatic departure term was computed for each trajectory. In the bulk of the cases both kinematic and isentropic results were comparable, indicating a trajectory accuracy to only 5°K. Only in the largest category of vertical departure did the kinematic trajectory show an improvement over the isentropic method. However, the departure was over 10°K and all methods are suspect in these complex situations.

A comparison of the trajectories with concurrent CO measurements at Chebogue indicated that there were natural trajectory clusters based primarily upon temporal homogeneity in the flow. Easterly flow from the ocean was associated with the smallest CO values, while southwest flow had the highest CO measurements. However, single peak concentrations seemed more likely to be associated with transitions from one homogeneous flow regime to another, those same baroclinic situations that produced the largest vertical displacements between the kinematic and isentropic approaches, suggesting extreme caution when attributing a measurement event to a single trajectory.

Acknowledgments. Partial support for this research has been provided by the Atmospheric Chemistry Project of the NOAA Climate and Global Change Program.

References

Artz, R., R.A. Pielke, and J. Galloway, Comparison of the ARL/ATAD constant level and the NCAR isentropic trajectory analyses for selected case studies, *Atmos. Environ., 19*, 47-63,

1985.

Akeredolu, F.A., L.A. Barrie, M.P. Olson, K.K. Oikawa, J.M. Pacyna, and G.J. Keeler, The flux of anthropogenic trace metals into the Arctic from the mid-latitudes in 1979/80, *Atmos. Environ., 28*, 1557-1572, 1994.

Andreae, M.O., B.E. Anderson, D.R. Blake, J.D. Bradshaw, J.E. Collins, G.L. Gregory, G.W. Sachse, and M.C. Shipham, Influence of plumes from biomass burning on atmospheric chemistry over the equatorial and tropical South Atlantic during CITE3, *J. Geophys. Res., 99*, 12,793-12,808, 1994.

Cheng, M.-D., P.K. Hopke, and Y. Zeng, A receptor-oriented methodology for determining source regions of particulate sulfate observed at Dorset, Ontario,*J. Geophys. Res., 98,* 16,839-16,849, 1993.

Danielsen, E.F., Trajectories: Isobaric, isentropic, and actual, *J. Meteorol., 18*, 479-486, 1961.

Draxler, R.R., Hybrid single particle Lagrangian integrated trajectories (HY-SPLIT)" Version 3.0 -- User's guide and model description, *NOAA Tech. Memo. ERL ARL-195*, 26 pp., with appendices, Natl. Tech. Info. Serv., Springfield, Va., 1992.

Fehsenfeld, F.C, S. Penkett, M. Trainer, and D.D. Parrish, NARE 1993 Summer Intensive: Foreward, *J. Geophys. Res.*, this issue

Ferber, G.J., J.L. Heffter, R.R. Draxler, R.J. Lagomarsino, F.L. Thomas, R.N. Dietz, and C.M. Benkovitz, Cross Appalachian tracer experiment (CAPTEX-83) Final Rep.,*NOAA Tech. Memo., ERL ARL-142*, Air Resour. Lab., Silver Spring, Md., 1986.

Fontan, J., A. Druilhet, B. Benech, R. Lyra, and B. Cros, The DECAFE experiments: Overview and meteorology, *J. Geophys. Res., 97*, 6123-6136, 1992.

Haagenson, P.L., K. Gao, and Y.-H. Kuo, Evaluation of meteorological analyses, simulations, and long-range transport calculations using ANATEX surface tracer data, *J. Appl. Meteorol., 29*, 1268-1283, 1990

Haagenson, P.L., and P.D. Sperry, A relationship of isentropic back trajectories with observed wind direction and synoptic type in the North Atlantic, *J. Appl. Meteorol., 28*, 25-42, 1989.

Hahn, C.J., J.T. Merrill, and B.G. Mendonca, Meteorological Influences during MLOPEX,*J. Geophys. Res., 97*, 10291-10309, 1992.

Harris, J., An analysis of 5-day midtropospheric flow patterns for the South Pole: 1985-1989, *Tellus, 44*B, 409-421, 1992.

Kuo, Y.-H., M. Skumanich, P.L. Haagenson, and J.S. Chang, The accuracy of trajectory models as revealed by the observing system simulation experiments, *Mon. Weather. Rev., 113*, 1852-1867, 1985.

Kahl, J.D., J.M. Harris, and G.A. Herbert, Intercomparison of three long-range trajectory models applied to Arctic haze, *Tellus, 41*B, 524-536, 1989.

Klemm, O., A.S. Bachmeier, R.W. Talbot, and K.I. Klemm, Fog chemistry at the New England coast: Influence of air mass history, *Atmos. Environ., 28*, 1181-1188, 1994.

Knudsen, B.M., and G.D. Carver, Accuracy of the isentropic trajectories calculated for the EASOE campaign, *Geophys. Res. Let., 21*, 1199-1202, 1994.

Lee, G., J.T. Merrill, and B.J. Huebert, Variation of free tropospheric total nitrate at Mauna Loa Observatory, Hawaii, *J. Geophys. Res., 99*, 12,821-12,831, 1994.

Lowenthal, D.H., R.D. Borys, J.C. Chow, F. Rogers, and G.E. Shaw, Evidence for long-range transport of aerosol from the Kuwaiti oil

fires to Hawaii, *J. Geophys. Res., 97*, 14,573-14,580, 1992.
Martin, D., C. Mithieux, and B. Strauss, On the use of the synoptic vertical wind component in a transport trajectory model, *Atmos. Environ., 21*, 45-52, 1987.
Merrill, J.T., R. Bleck, and D. Boudra, Techniques of Lagrangian trajectory analysis in isentropic coordinates, *Mon. Weather. Rev., 114*, 571-581, 1986.
Moody, J.L., and J.N. Galloway, Quantifying the relationship between atmospheric transport and the chemical composition of precipitation on Bermuda, *Tellus, 40*B, 463-479, 1988.
Moody, J.L., and P.J. Samson, The influence of atmospheric transport on precipitation chemistry at two sites in the Midwestern United States, *Atmos. Environ., 23*, 2117-2132, 1989.
Moy, L.A., R.R. Dickerson, and W.F. Ryan, Relationship between back trajectories and tropospheric trace gas concentrations in rural Virginia, *Atmos. Environ., 28*, 2789-2800, 1994.
Mueller, S.F., Characterization of ambient ozone levels in the Great Smoky Mountains National Park, *J. Appl. Meteorol., 33*, 465-472, 1994.
Mukai, H., A. Tanaka, and T. Fujii, Lead isotope ratios of airborne particulate matter as tracers of long-range transport of air pollutants around Japan, *J. Geophys. Res., 99*, 3717-3726, 1994.
Oltmans, S., and H. Levy II, Surface ozone measurements from a global network, *Atmos. Environ., 28*, 9-24, 1994.
Olson, M.P., and K.K. Oikawa, Interannual variability of transboundary sulphur flux, *Atmos. Environ., 23*, 333-340, 1989.
Oram, D.E., and S.A. Penkett, Observations in eastern England of elevated methyl iodide concentrations in air of Atlantic origin, *Atmos. Environ., 28*, 1159-1174, 1994.
Paluch, I.R., D.H. Lenschow, J.G. Hudson, and R. Pearson, Jr., Transport and mixing processes in the lower troposphere over the ocean, *J. Geophys. Res., 97*, 7527-7541, 1992.
Pickering, K.E., A.M. Thompson, D.P. McNamara, and M.R. Schoeberl, An intercomparison of isentropic trajectories over the South Atlantic, *Mon. Weather. Rev., 122*, 864-879, 1994.
Roberts, J.M., et al., Episodic removal of NO_y species from the marine boundary layer over the North Atlantic, *J. Geophys. Res.*, this issue
Shipman, M.C., A.S. Bachmeier, D.R. Cahoon, and E.V. Browell, Meteorological overview of the Arctic boundary layer expedition (ABLE 3A) Flight Series, *J. Geophys. Res., 97*, 16,395-16,419, 1992.
Stohl, A., and H. Kromp-Kolb, Origin of ozone in Vienna and surroundings, Austria, *Atmos. Environ., 28*, 1255-1266, 1994.
Stunder, B.J.B., R.S. Artz, G.D. Rolph, J.M. Harris, and J.T. Merrill, Summary of meteorological conditions over the North Atlantic Ocean during GCE/CASE/WATOX, *Global Biogeochem. Cycles, 4*, 133-150, 1990.
Swap, R., M. Garstang, S. Greco, R. Talbot, and P. Kållberg, Saharan dust in the Amazon Basin, *Tellus, 44*B, 133-149, 1992.
Taguchi, S., Cross-tropical trajectories in the troposphere, *J. Meteorol. Soc. Jpn., 72*, 531-553, 1994

R.R. Draxler, NOAA, Air Resources Laboratory, 1315 East West Highway, Silver Spring, MD 20910. (e-mail: roland.draxler@noaa.gov)

(Received May 25, 1995; revised October 24, 1995;
accepted November 28, 1995.)

Paper number 95JD03760.
0148-0227/96/955D-03760$05.00

Table 1. The Three Independent Meteorological Periods (A,C,D) with Kinematic-Isentropic Trajectory Pairs With Large Vertical Displacements.

Period	Date	Trajectories Starting Times (UTC)
A	Aug. 6	0000, 0600, 1200, 1800
	Aug. 7	0000
C	Aug. 22	0000, 0600
D	Aug. 29	0600, 1200

The periods also refer to the panel labels of Figure 7.

Table 2. Average CO Air Concentration Associated With Each Trajectory Period and Upwind Direction.

Period	Start Day UTC	End Day UTC	Upwind Direction	CO Level ppb	Sigma ppb
1	1 1000	5 1800	SW	140.2	17.2
2	6 0000	9 1800	NW/SW/E	133.4	23.1
3	11 0000	14 1800	E	106.3	5.8
4	15 0000	17 1800	N	141.8	9.2
5	18 0000	21 1800	SE	113.6	7.7
6	22 0000	26 0000	SW to NW	116.4	28.8
7	26 0000	28 0000	NW	168.1	32.8
8	28 0600	29 0000	SW	170.6	51.4
9	29 0600	31 1800	NW	122.8	23.1

Trajectory dates are for August with the times indicated as hour UTC.

Figure 1. Relative Horizontal Trajectory Difference (RHTD) between the isentropic and kinematic calculations as a function of their vertical displacement from each other averaged into 25-hPa bins.

Figure 2. Number of trajectories within each vertical displacement bin at intervals of 25 hPa.

Figure 3. Kinematic trajectories for August 1993 for which the vertical displacement between the corresponding isentropic calculation is less than 100 hPa.

Figure 4. August 1993 isentropic trajectories corresponding to the same low vertical displacement cases shown in Figure 3.

Figure 5. The few kinematic trajectories during August 1993 where the vertical displacements between the corresponding isentropic cases is greater than 100 hPa.

Figure 6. The isentropic trajectories for the same high displacement cases as shown in Figure 5.

Figure 7. Mean sea level pressure (hPa) for (a) August 6 0000 UTC, (b) August 7 0000 UTC, (c) August 22 0000 UTC, and (d) August 29 0600 UTC.

Figure 8. The kinematic isentropic trajectory pair starting August 22 1200 UTC, 6 hours after the end of the high dis-

placement period.

Figure 9. The kinematic isentropic trajectory pair starting August 29 1800 UTC, 6 hours after the end of the high displacement period.

Figure 10. Isentropic trajectory (crosses) starting at August 22 0000 UTC, at the beginning of the large vertical displacement period. Contours show the potential temperature (°K) surfaces along the trajectory path.

Figure 11. Isentropic trajectory (crosses) starting 12 hours after the one shown in Figure 10, and the same as shown in Figure 8. Contours show potential temperature surfaces (°K).

Figure 12. Isentropic trajectory (crosses) starting August 29 0600 UTC, at the beginning of the large displacement period. Contours show the potential temperature surfaces (°K).

Figure 13. Isentropic trajectory (crosses) starting 12 hours after the one in Figure 12, and the same as shown in Figure 9. Contours show the potential temperature surfaces (°K).

Figure 14. Average difference in the energy balance between the kinematic and isentropic trajectories expressed in degrees by vertical displacement category.

Figure 15. Average 6-hour CO concentrations centered about the trajectory starting times at Chebogue for August of 1993. Vertical dotted lines indicate transitions between different flow regimes.

Figure 16. The average trajectory for each of the nine periods. Trajectories are marked by the period identification at 6-hour intervals.

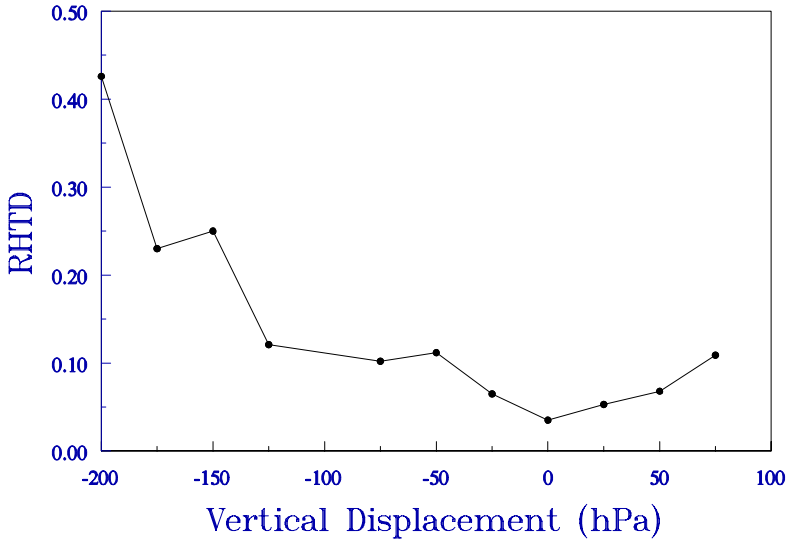
0.50
0.40
0.30
0.20
0.10
0.00
RHTD
-200
-150
-100
-50
0
50
100
Vertical Displacement (hPa)

Figure 1.

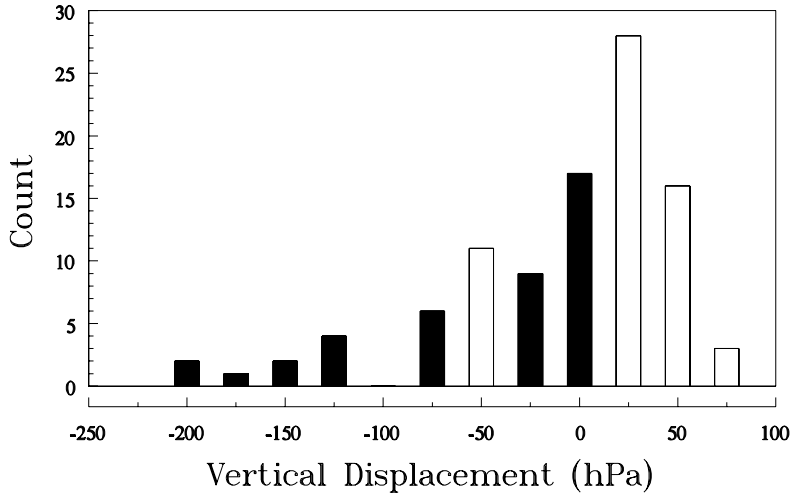
30
25
20
15
10
5
0
Count
-250
-200
-150
-100
-50
0
50
100
Vertical Displacement (hPa)

Figure 2.

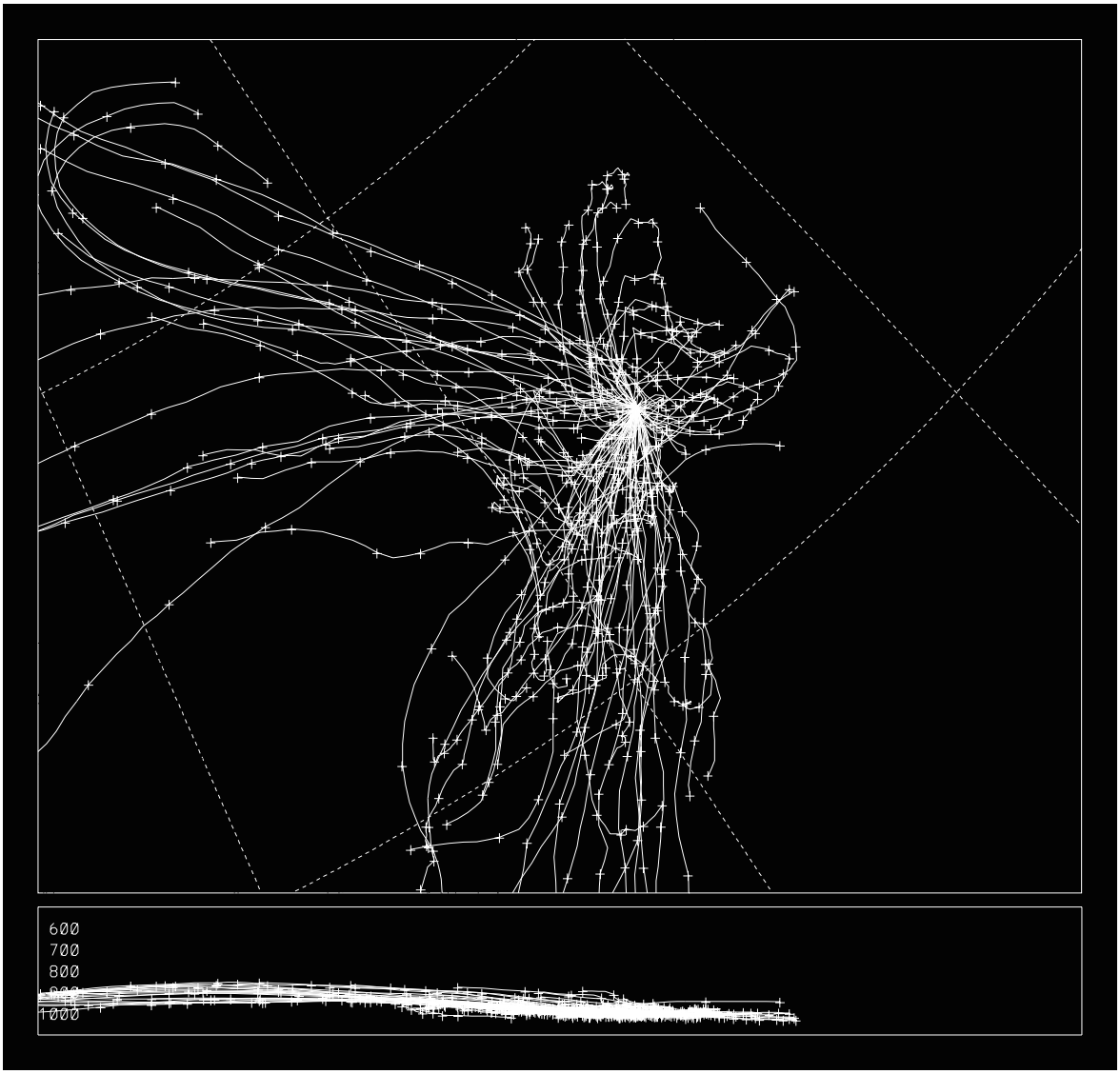

Figure 3.

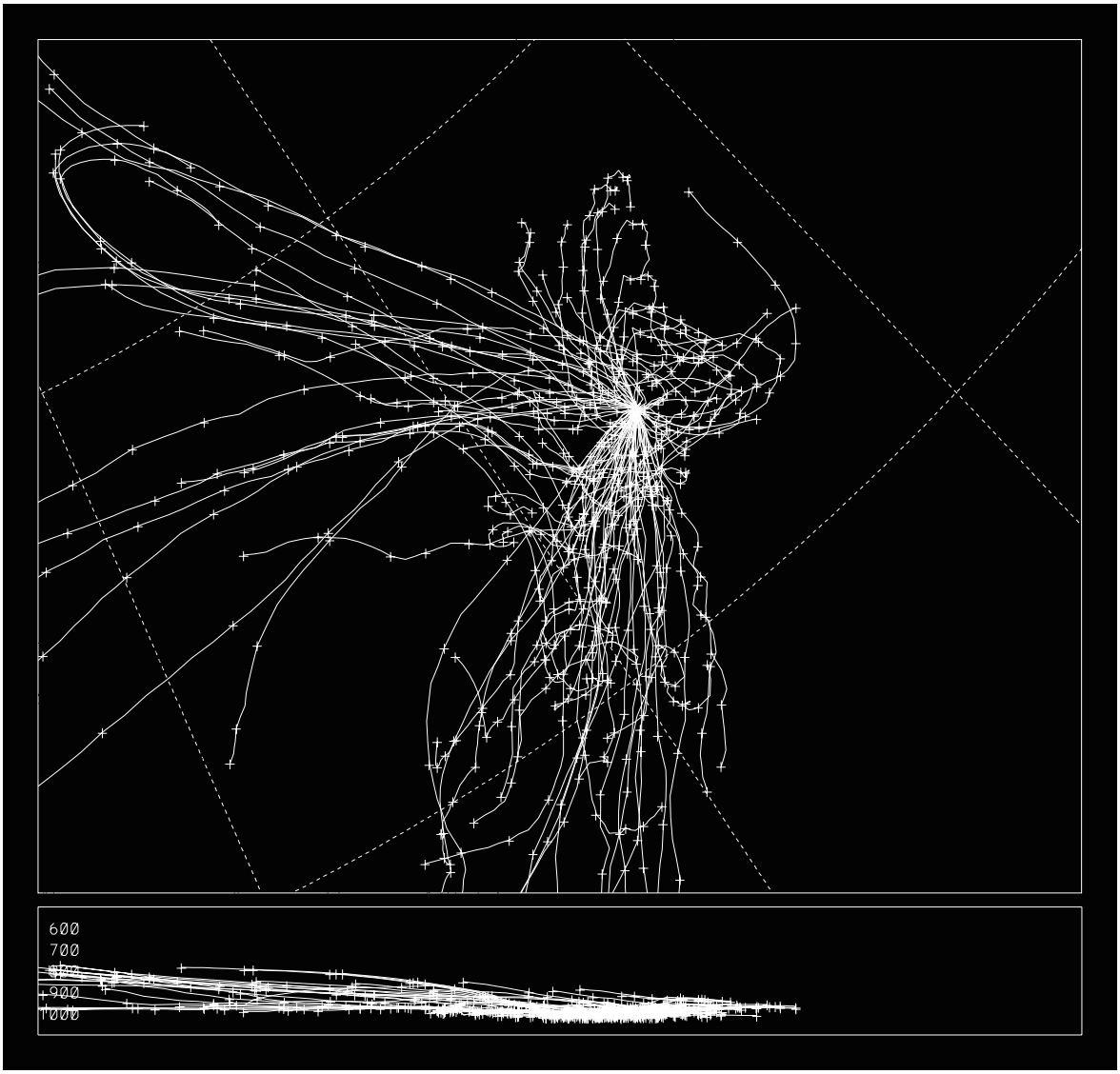

Figure 4.

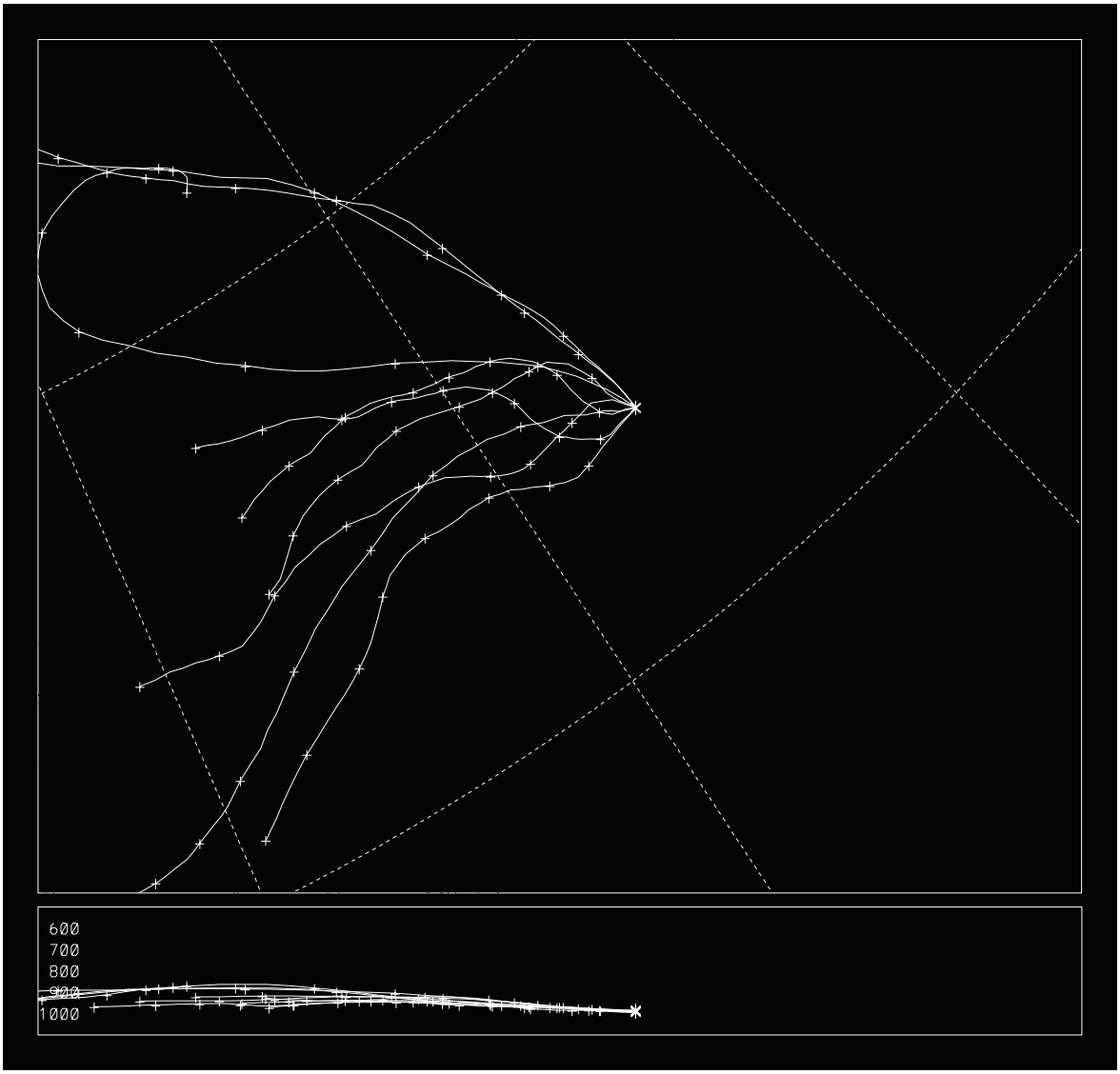

Figure 5.

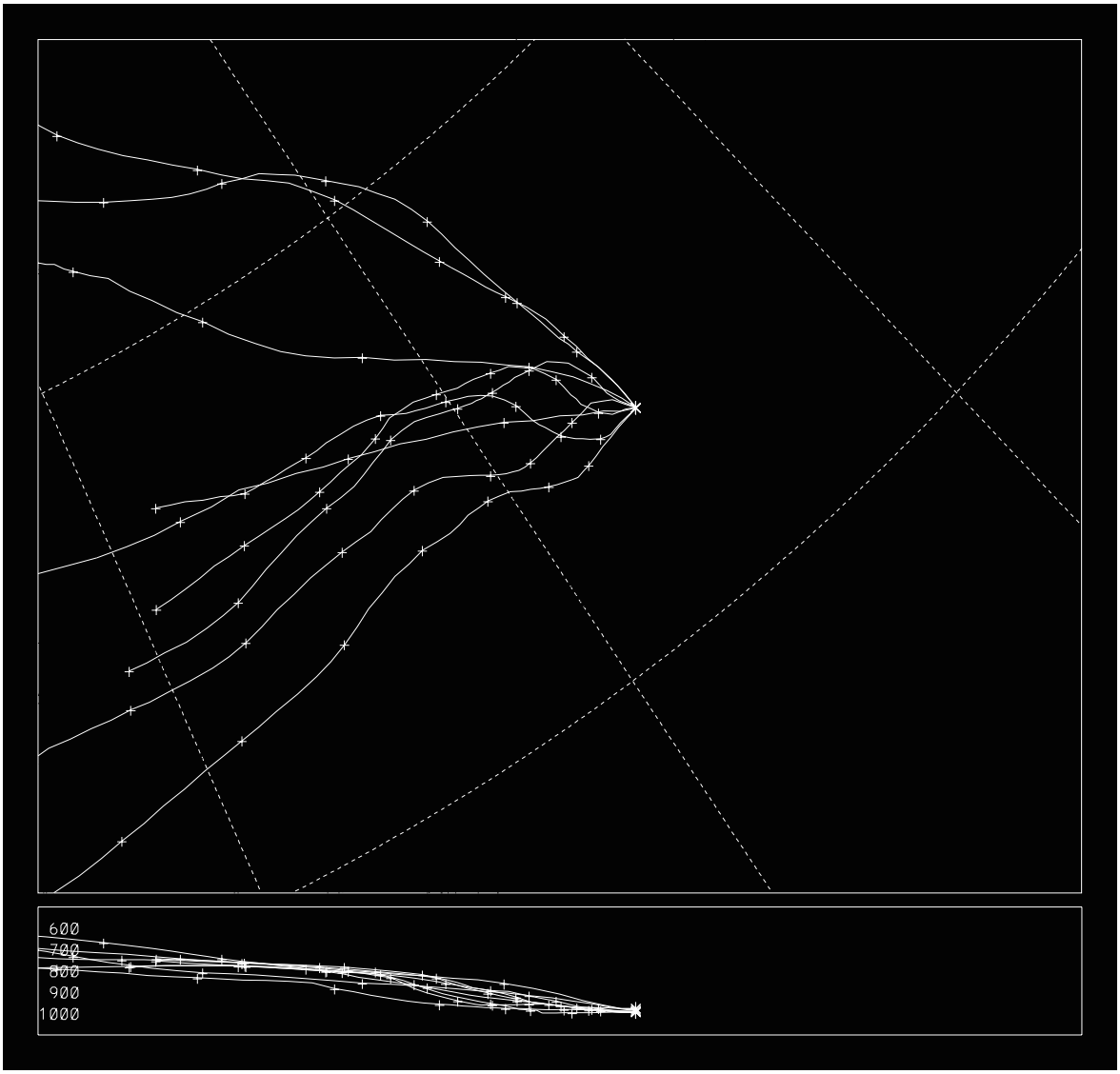

Figure 6.

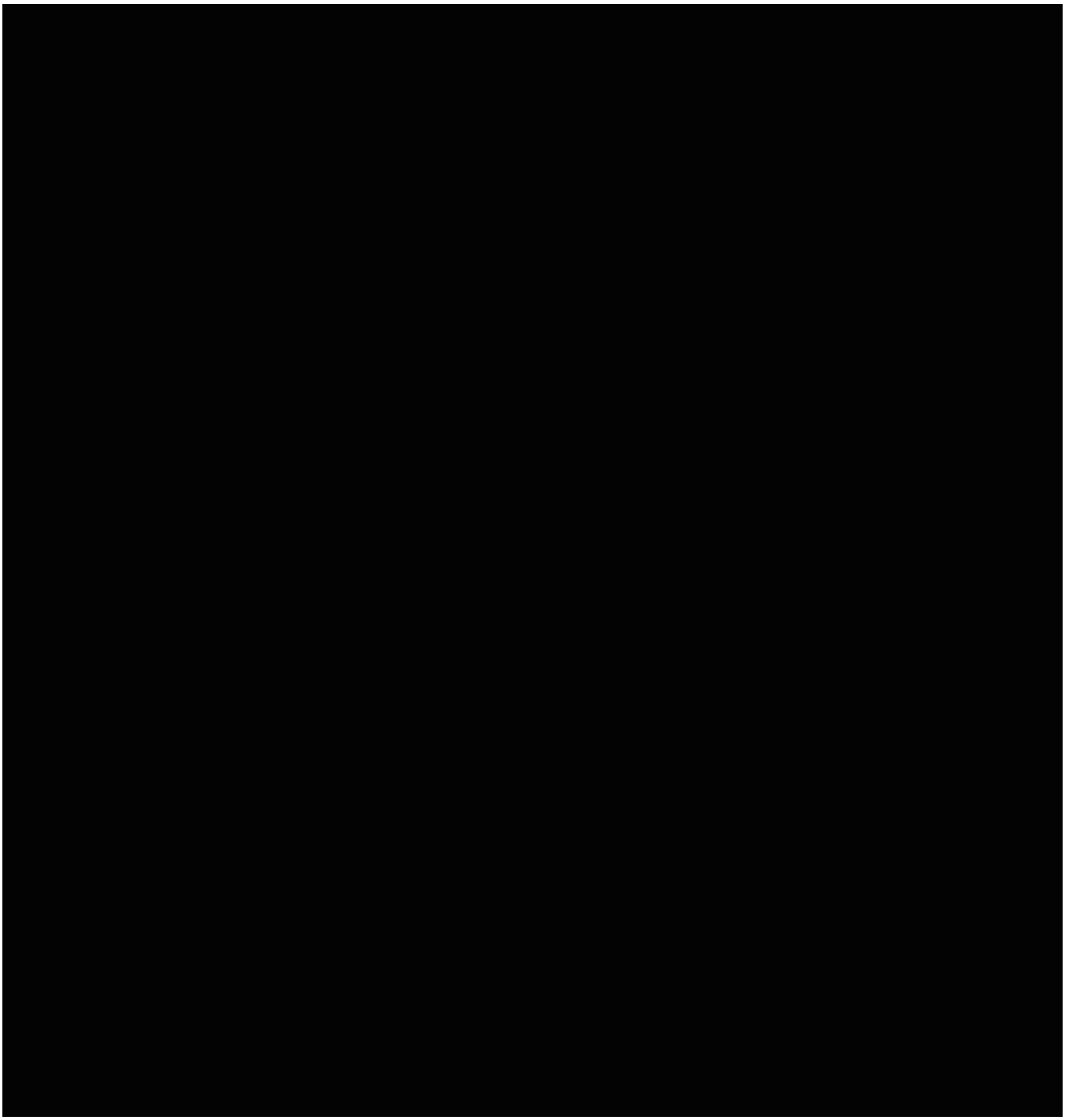

Figure 7.

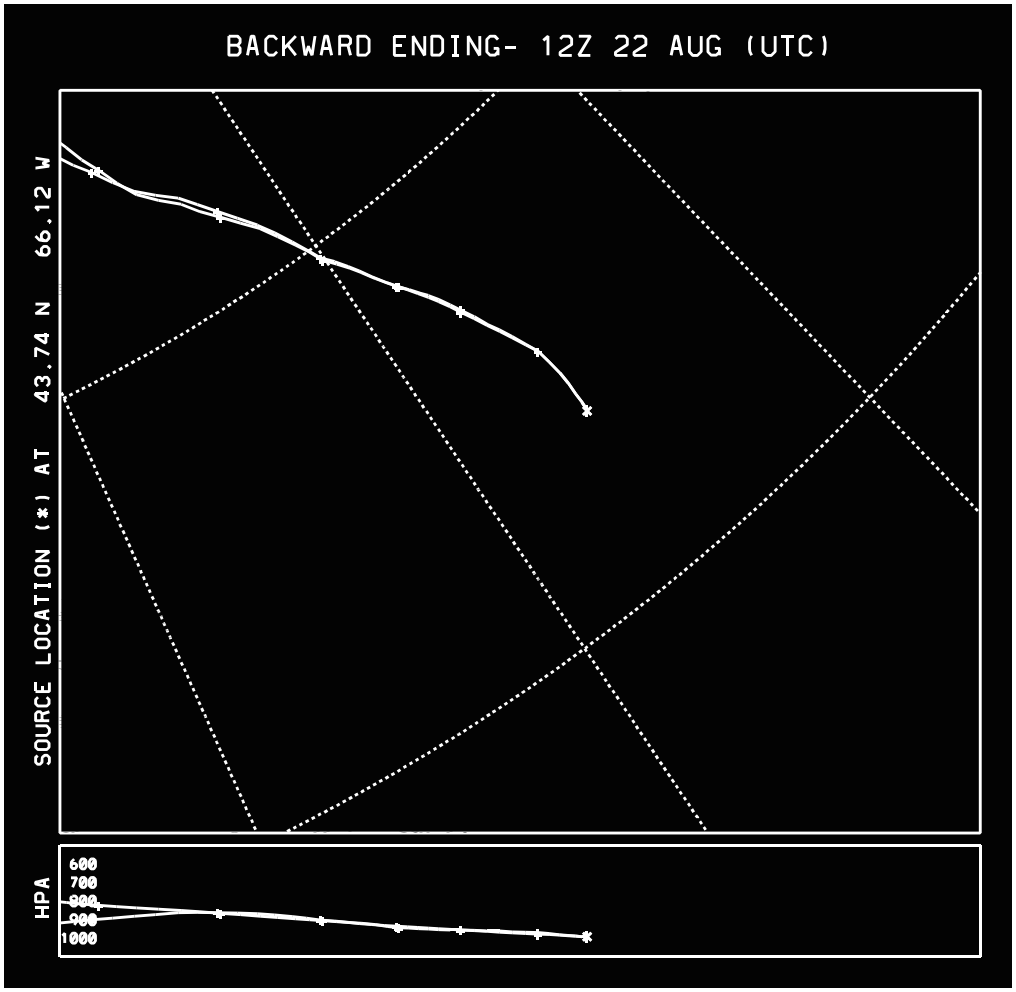
BACKWARD ENDING- 12Z 22 AUG (UTC)
SOURCE LOCATION (*) AT 43.74 N 66.12 W
HPA
600
700
800
900
1000

Figure 8.

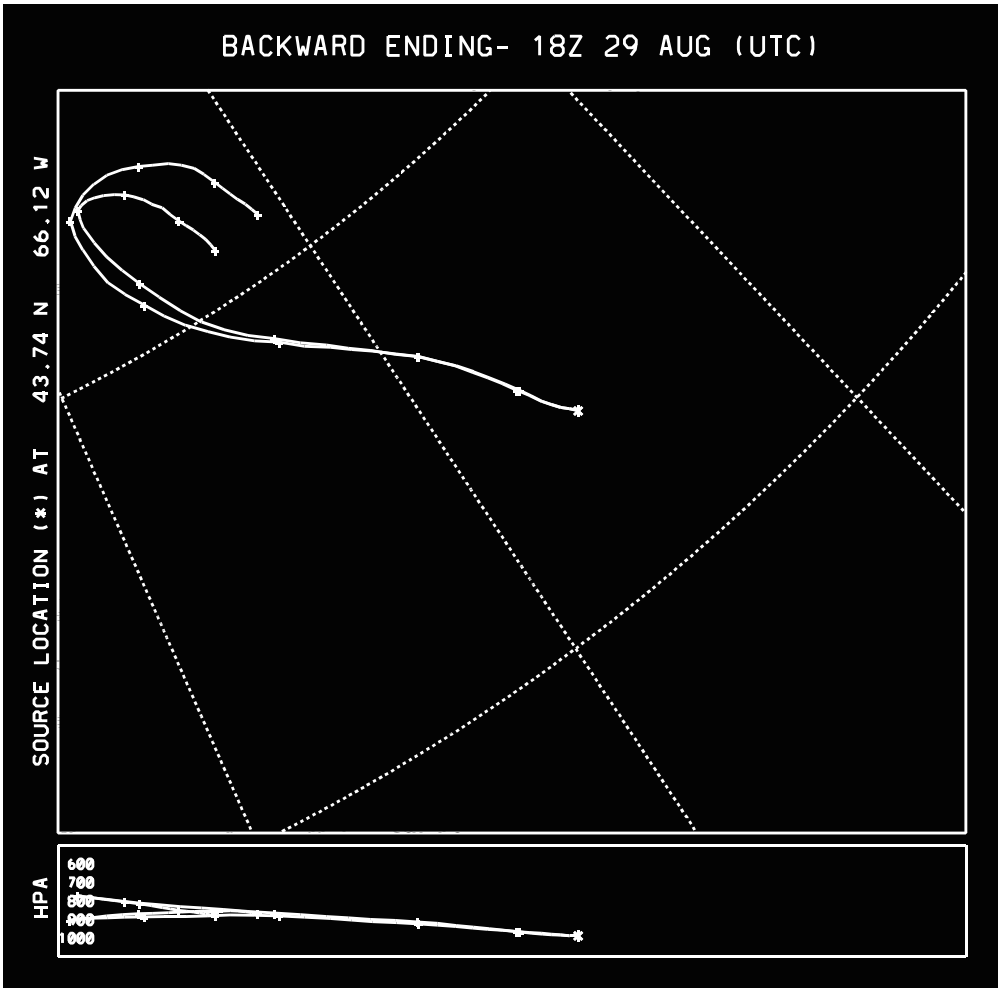
BACKWARD ENDING- 18Z 29 AUG (UTC)
SOURCE LOCATION (*) AT 43.74 N 66.12 W
HPA
600
700
800
900
1000

Figure 9.

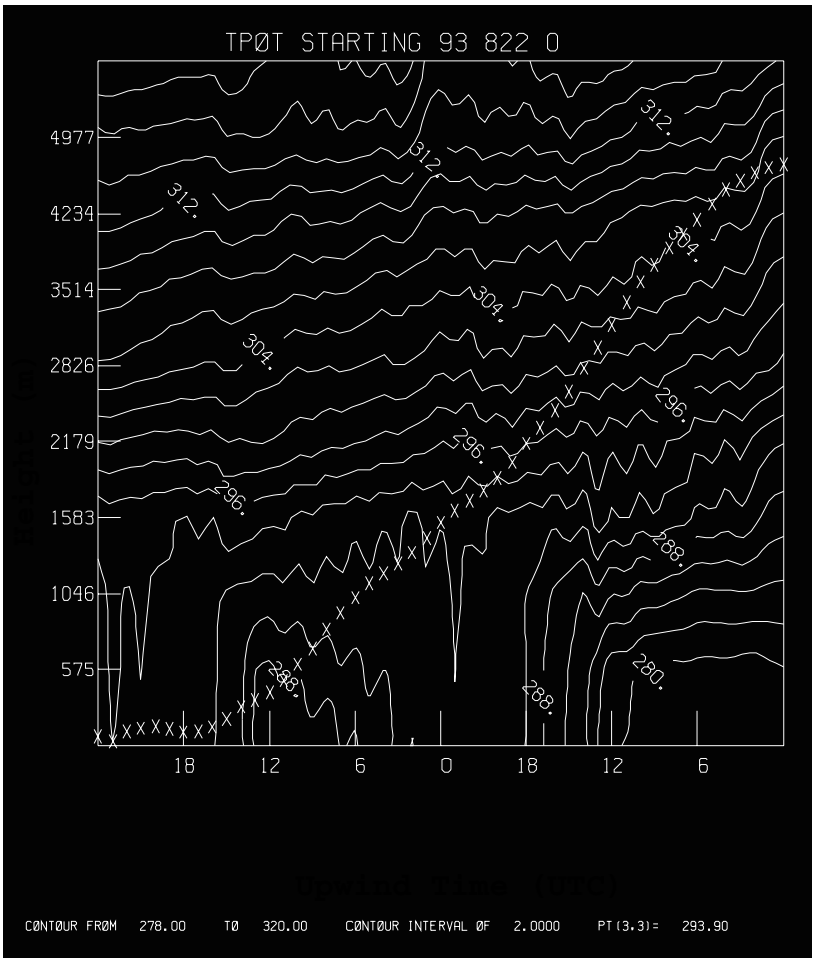
TPØT STARTING 93 822 0
4977
4234
3514
2826
2179
1583
1046
575
312.
304.
296.
288.
280.
18
12
6
0
18
12
6
CØNTØUR FRØM 278.00 TØ 320.00 CØNTØUR INTERVAL ØF 2.0000 PT(3,3)= 293.90

Figure 10.

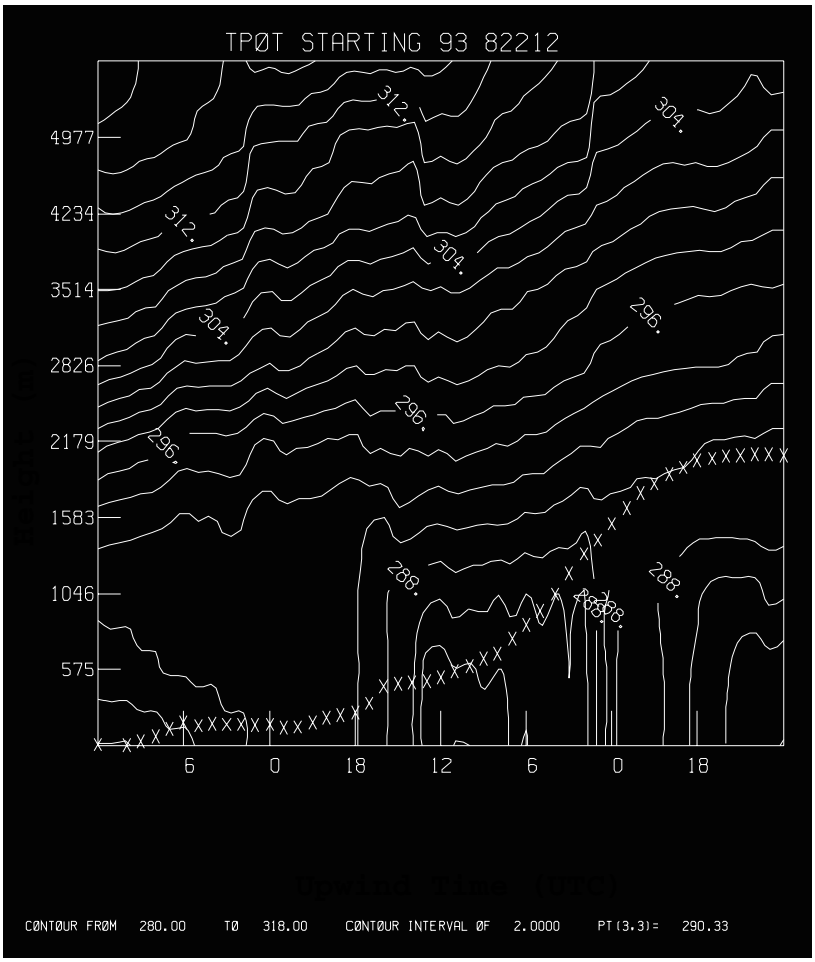
TPØT STARTING 93 82212
4977
4234
3514
2826
2179
1583
1046
575
312.
304.
296.
288.
6
0
18
12
6
0
18
CØNTØUR FRØM 280.00 TØ 318.00 CØNTØUR INTERVAL ØF 2.0000 PT(3,3)= 290.33

Figure 11.

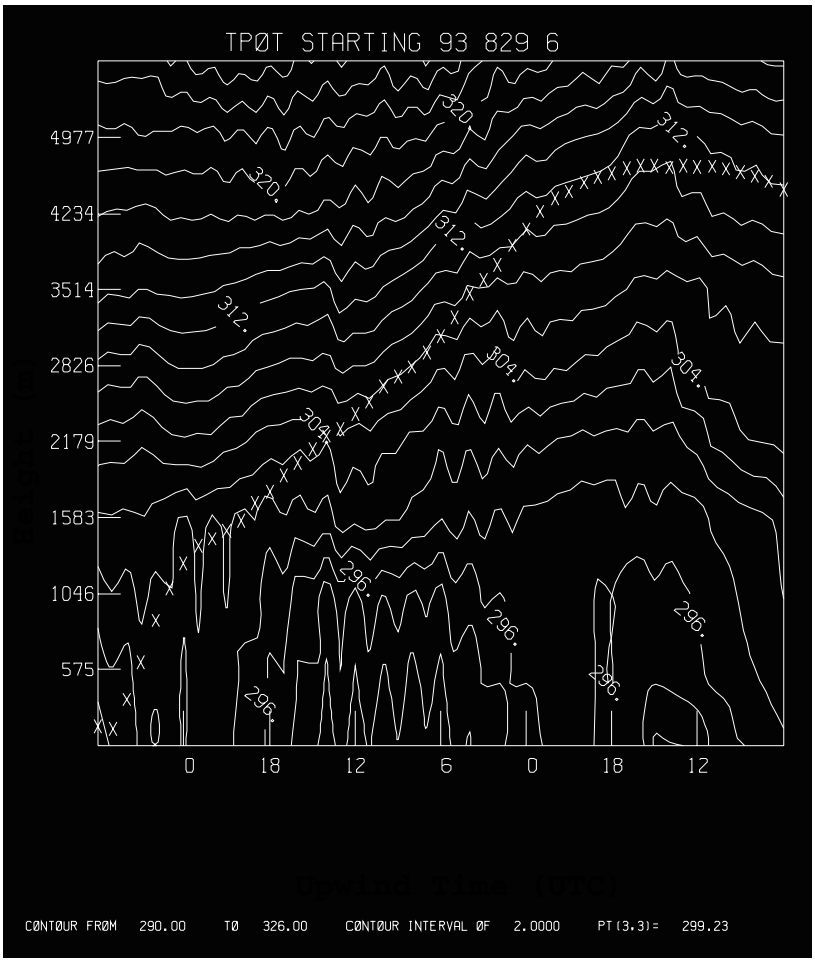
TPØT STARTING 93 829 6
4977
4234
3514
2826
2179
1583
1046
575
320.
312.
304.
296.
0
18
12
6
0
18
12
Upwind Time (UTC)
CØNTØUR FRØM 290.00 TØ 326.00 CØNTØUR INTERVAL ØF 2.0000 PT(3,3)= 299.23

Figure 12.

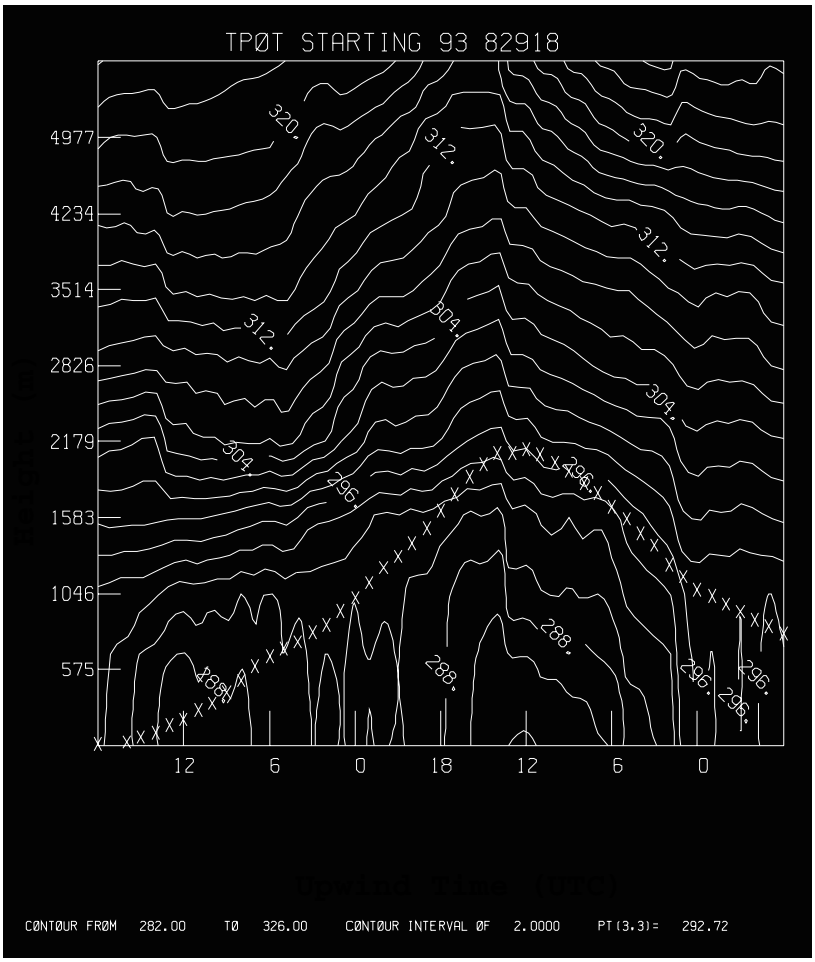
TPØT STARTING 93 82918
4977
4234
3514
2826
2179
1583
1046
575
320.
312.
304.
296.
288.
12
6
0
18
12
6
0
Upwind Time (UTC)
CØNTØUR FRØM 282.00 TØ 326.00 CØNTØUR INTERVAL ØF 2.0000 PT(3,3)= 292.72

Figure 13.

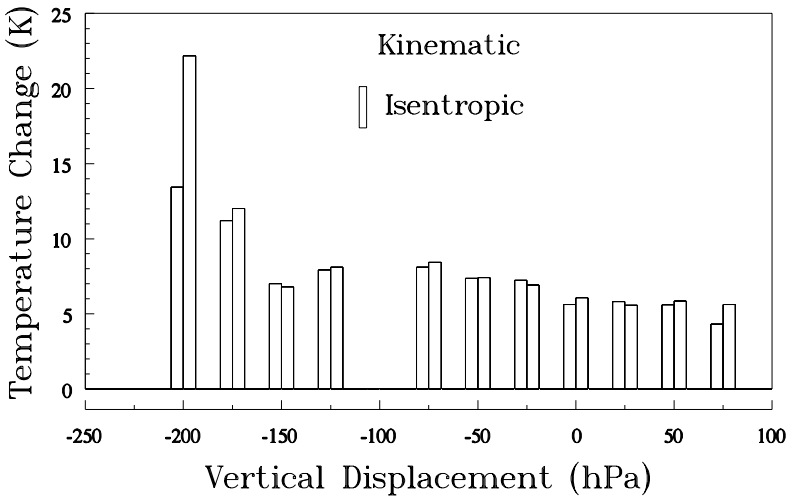
Kinematic
Isentropic
Temperature Change (K)
25
20
15
10
5
0
-250
-200
-150
-100
-50
0
50
100
Vertical Displacement (hPa)

Figure 14.

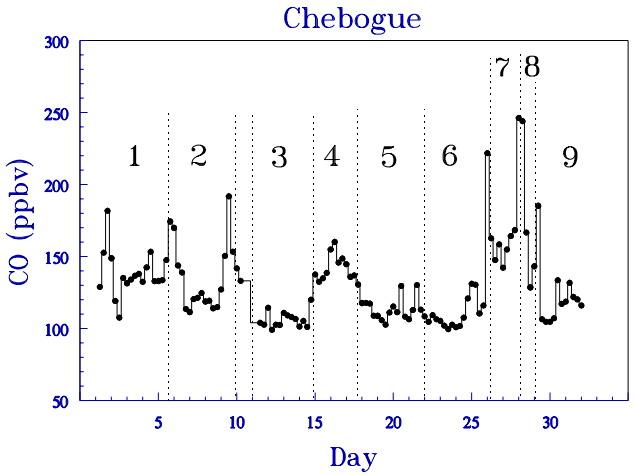
Chebogue
CO (ppbv)
Day
300
250
200
150
100
50
5
10
15
20
25
30
1
2
3
4
5
6
7
8
9

Figure 15.

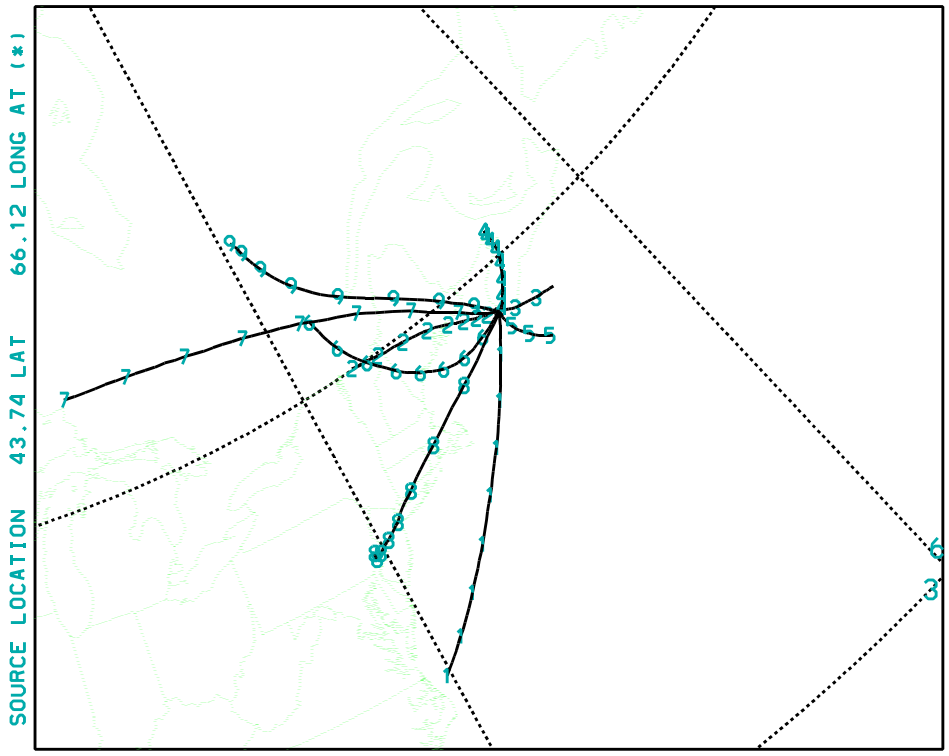

Figure 16.